Manufacturing and Testing a Finger Seal and Comparison with Reduced Order Models

Eli Smith[1], Sean Magoffin[2], Cody Greener[3], and Matthew S. Allen[4]

[1]Undergraduate Research Assistant, Brigham Young University, Department of Mechanical Engineering, es487@byu.edu
[2]Undergraduate Research Assistant, Brigham Young University, Department of Mechanical Engineering, sm996@byu.edu
[3]Graduate Research Assistant, Brigham Young University, Department of Mechanical Engineering, grecody@byu.edu
[4]Professor, Brigham Young University, Department of Mechanical Engineering, matt.allen@byu.edu

Abstract

Finger seals are an innovative solution for sealing in environments where conventional seals fail due to extreme longevity requirements or high temperatures. While prior research has primarily focused on the thermal and fluid flow characteristics of finger seals, their influence on structural dynamics remains largely unexplored. This paper investigates the dynamic behavior of a finger seal-like structure consisting of two beams arranged like a tuning fork, with a curved sheet metal element compressed between them. Impact testing was performed to measure the structure's dynamic responses, and the Hilbert transform was employed to characterize the nonlinear dynamics across the first few vibration modes. The results reveal significant changes in modal behavior as the structure transitions from micro-slip to macro-slip with increasing amplitude. A reduced-order model was created by applying the Hurty/Craig-Bampton reduction technique to a finite element model with spiders used to reduce each interface to a pair of nodes. Iwan elements were then inserted between the interface nodes, and quasi-static modal analysis was used to tune the model to reproduce the dynamics of the measured modes.

Keywords: Iwan Joint, Finger Seal, Nonlinearity, Friction

1 Introduction

Secondary airflow in gas turbine engines is used for cooling, operation, and engine efficiency. Seals are required to maintain a separation between the secondary and primary airflow in the engine. Improving the effectiveness of the seals is a classical way of improving the efficiency and longevity of an engine [1]. Novel seal designs and materials are required in situations where the longevity and temperature requirements of the engine necessitate it, such as in gas turbine engines. Seal designs such as W-seals, feather seals, and dog-bone seals can be used to interface and maintain pressure differences at various locations in an engine [1]. However, these designs are prone to damage during engine assembly and operation [1].

Another approach, sometimes referred to as a finger seal, involves using a curved piece of sheet metal under compression against a stiff, unyielding surface [1, 2]. The design is comparable to the metallic seals in [3]. This study focuses on the effect of these seals on the dynamics of the structure, and in particular on energy loss due to damping. It is worth noting that a distinctly different type of seal, designed for use around a rotating or stationary shaft, is also known as a finger seal. It is discussed in the "Finger Seal" section of [3], but is distinct from the seal type that is the focus of this paper [1, 2].

Several advances have been made in recent years in our understanding of bolted joints and their influence on structural vibrations [4, 5, 6]. One approach that has gained some traction involves inserting Iwan elements between interface nodes in a finite element and then using quasi-static modal analysis to predict their effect on the damping of the modes of interest [7, 8].

This study aims to characterize the dynamics of a finger seal through experimental testing on a finger seal-like test structure. Roving hammer testing was conducted to find the natural frequencies and damping ratios as a function of vibration amplitude for all of the lower-order modes of the system. The experimental results are used to develop both a linear reduced order model (ROM) and a nonlinear ROM using Iwan Elements and the Quasi-Static Modal Analysis (QSMA) method as in [7]. It is worth noting that there is at least one other work that has studied a similar structure. In [9], thin strips of sheet metal were inserted in hollow cavities within beams representing turbine airfoils in order to enhance the damping.

The following section describes the design of the finger seal test stand and the experiments that were performed to characterize its linear and nonlinear dynamic behavior. Section 2.3 then describes the models that were created to capture its behavior.

Section 3 presents the results of the testing and model updating that was performed to identify Iwan parameters that brought the model into agreement with measurements. A companion paper elaborates more on the design of the test stand and discusses efforts to predict the nonlinear behavior of the finger seal using Finite Element Analysis with contact and Coulomb friction at the interfaces [10].

2 Methods

2.1 Dynamic Testing

A test stand was designed to approximate a finger seal as used in turbine engines [2], while also being simple enough to facilitate testing and modeling. The assembly consisted of two beams bolted together at one end with a spacer between them. The dimensions of the beams are 6.5 in x 1.5 in x 0.125 in and the spacer is 1 in x 1.5 in x 0.125. The beams and the spacer are made of 303 stainless steel. The bolts are 5/16-24 stainless steel with a 25 N-m pre-load to minimize damping due to the bolted joint. These beams approximate the surfaces against which a finger seal presses within an engine. To approximate a finger seal, a 1.375 in wide wavy parallel made of 0.015 in thick spring steel was purchased. The ends were cut off so that it would come into contact with the structure at three points when inserted between the beams as shown in Fig. 1.

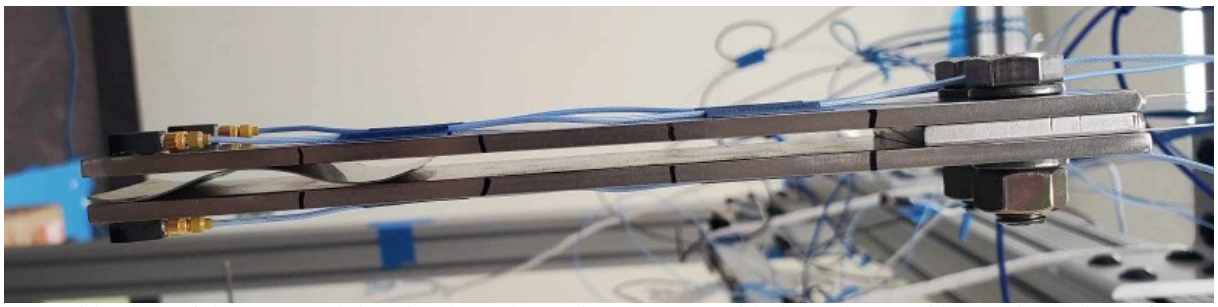

Figure 1: Side view of the test stand that simulates the engine structure with the spring steel insert simulating a finger seal.

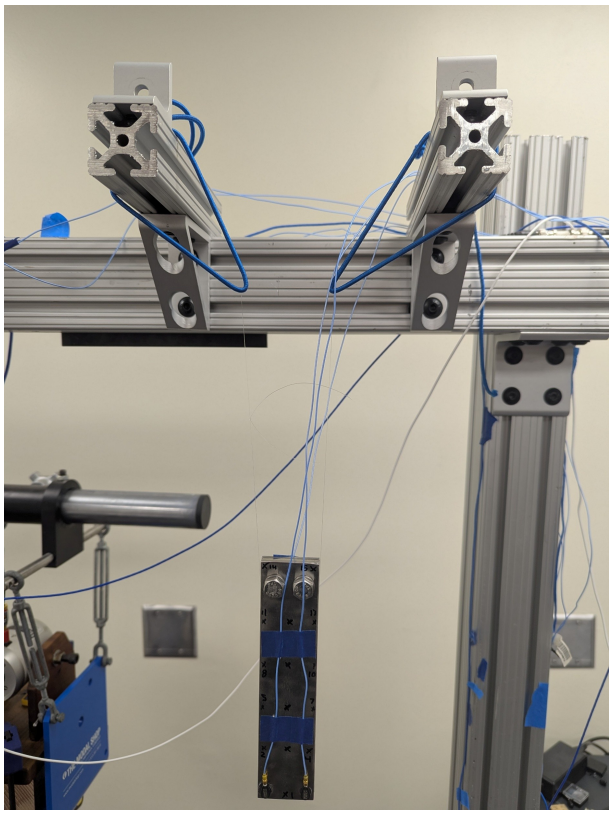

(a) Fishing line and blue bungee cords were used to simulate free boundary conditions.

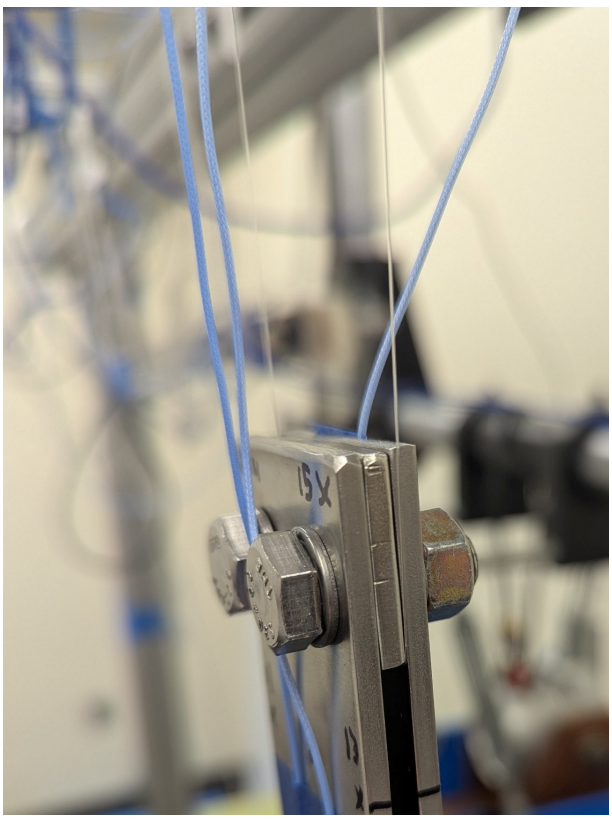

(b) Fishing Line Under Spacer

Figure 2: The test stand is suspended to simulate free boundary conditions.

Fishing line was looped through two bungee cords (Fig. 2a) and under the spacer (Fig. 2b) to suspend the test structure and simulate free boundary conditions. A total of thirty impact locations were marked with X's on the test stand, and four accelerometers were super-glued to the four outer corners of the test structure, opposite the bolts, with the positive direction normal to their respective outer faces as seen in Fig. 3. Linear and nonlinear roving hammer tests were used to capture the modes of the system.

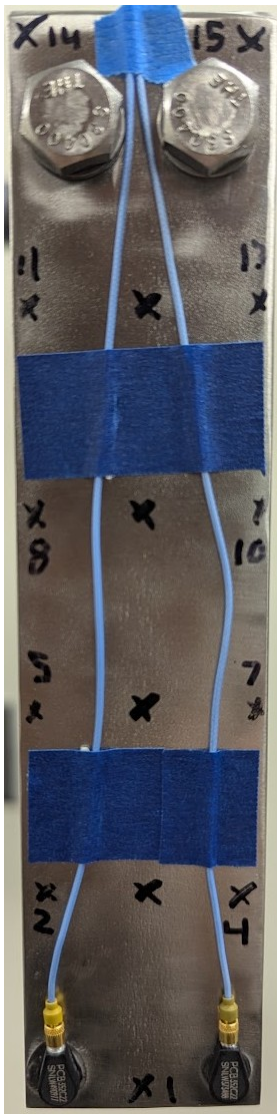

(a) Front Face, with accelerometer 1 on the left and 2 on the right.

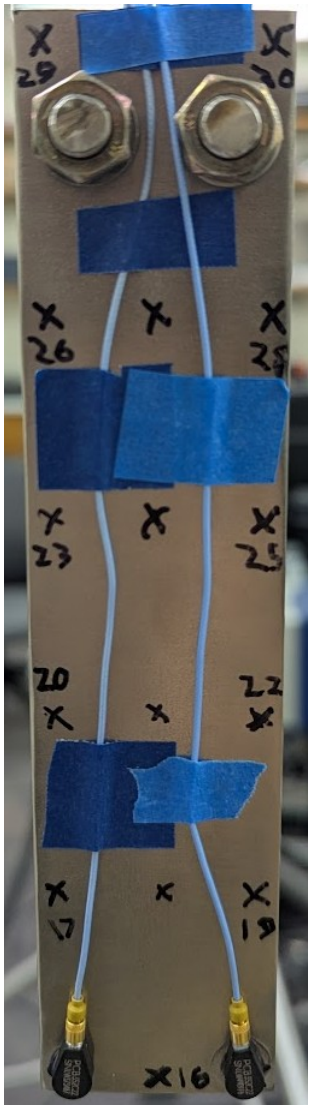

(b) Back Face, with accelerometer 4 on the left and 3 on the right.

Figure 3: Locations of accelerometers and impact points.

A small hammer (PCB Piezotronics Model 086E80) was used for the linear tests, with an impact range of approximately 1-5 Newtons. This involved hits at all 30 impact locations, both with and without the spring steel insert to capture the linear natural frequencies, linear damping ratios, and mode shapes. The system was measured without the seal present in order to understand the influence of the seal on the structure and to update the material properties in the finite element model, as described in [10].

Nonlinear tests were performed using a medium-sized impact hammer (PCB Piezotronics Model 086C03). It was found that using a rubber tip was best for exciting Modes 1-3 and a plastic tip excited Modes 4-5. The larger hammer size allowed for an excitation of higher amplitudes of vibration and a transition of the system to macro-slip.

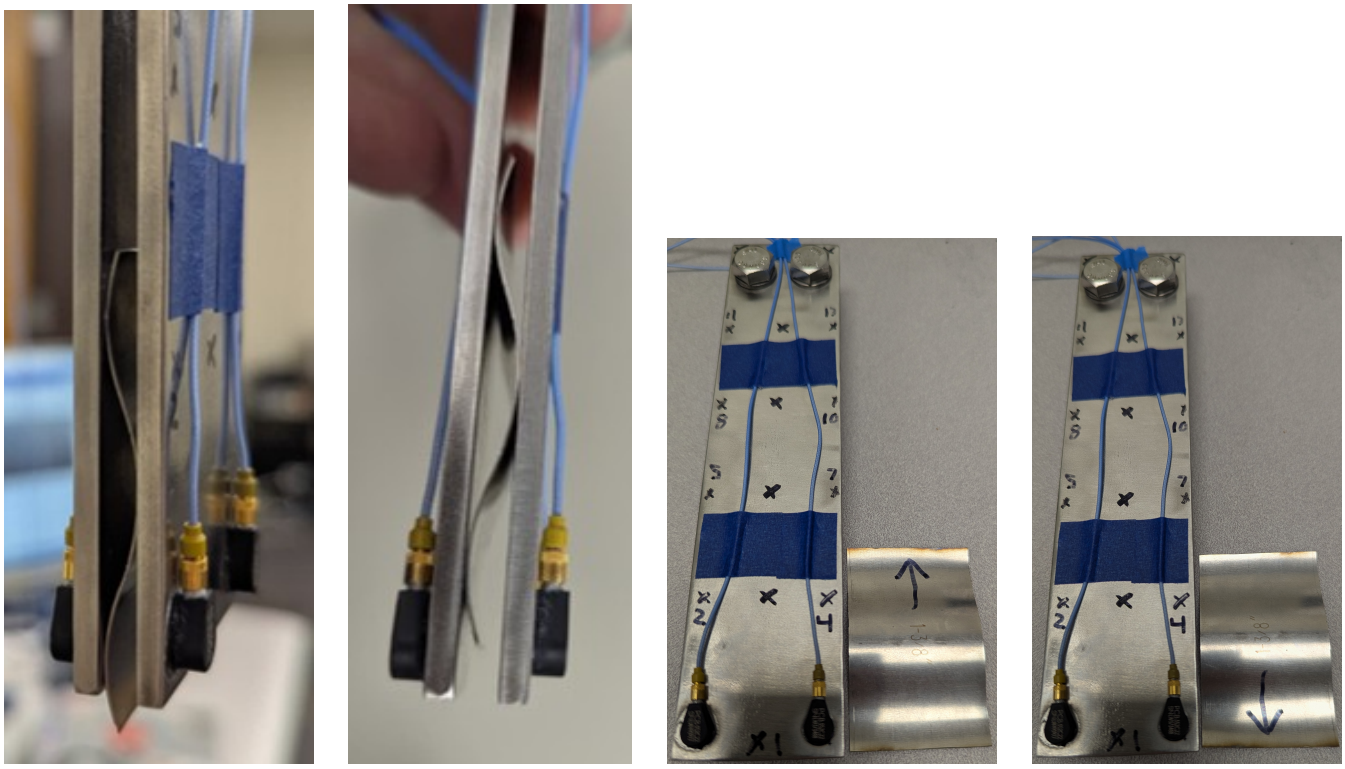

(a) Seal shifted down (b) Seal shifted up (c) Seal facing up (d) Seal facing down

Figure 4: Images of the seal for tests where the seal position was changed.

The orientation of the spring steel insert was varied to measure the sensitivity of the system to its position. The spring steel insert was shifted down and shifted up, which involved sliding the insert approximately 1/4 inch down (Fig. 4a) and up (Fig. 4b). While the spring steel insert appears to have a symmetrical geometry, its direction was changed (Figures 4c and 4d) and the tests repeated to quantify the degree to which any asymmetry in the seal affected the results.

2.2 Experimental Data Analysis

Acceleration data gathered from the small hammer impact tests was used to find natural frequencies, damping ratios, and mode shapes of the structure, both with and without the spring steel insert. A band-pass filter was combined with the Hilbert Transform to filter out the individual modes from the experimental throughput data, as was described in Gilbert et al. [11]. The mode frequencies exhibited a significant shift as the system transitioned from micro to macro-slip and exhibited strong nonlinearities. The four measured acceleration signals $a_1(t)$, $a_2(t)$, $a_3(t)$, and $a_4(t)$ (see Fig. 3 for their definitions) were combined as given in Eqs. (1a)-(1d),

$$y_{\text{sb}} = \tfrac{1}{4}(a_1(t) + a_2(t) + a_3(t) + a_4(t)) \tag{1a}$$

$$y_{\text{ab}} = \tfrac{1}{4}\left((a_1(t) + a_2(t)) - (a_3(t) + a_4(t))\right) \tag{1b}$$

$$y_{t1} = \tfrac{1}{4}\left((a_1(t) + a_4(t))(-1) + (a_2(t) + a_3(t))\right) \tag{1c}$$

$$y_{t2} = \tfrac{1}{4}\left((a_1(t) + a_3(t))(-1) + (a_2(t) + a_4(t))\right) \tag{1d}$$

to amplify the mode in question. These equations amplify the response of the symmetric bending mode (Eq. (1a)), the asymmetric bending mode (Eq. (1b)), the first torsional mode (Eq. (1c)), and the second torsional mode (Eq. (1d)). The equations have a scale factor of 4 so that their output has the same scale as any of the $a(t)$ signals. The variables $a_1(t)$ and $a_2(t)$ face the front and are shown in Fig. 3a, while $a_3(t)$ and $a_4(t)$ face the back and are shown in Fig. 3b. Symmetric vs asymmetric modes are defined by assuming that the spacer represents a dividing plane between the two beams. If the motion of the beams mirrored one another across that plane, then they were termed symmetric and if they do not mirror each other, then they were termed asymmetric.

The signals y_{sb}, y_{ab}, y_{t1}, and y_{t2} were processed using the Hilbert transform using the approach in [12, 11], resulting in graphs of the amplitude versus damping ratio and amplitude versus frequency of each mode at each hit point. The results from various hit points were combined to show the variation in the damping ratios and frequency of each mode of the structure.

2.3 Modeling

A 2D finite element model (FEM) was created in Abaqus and is outlined in a companion paper [10]. Multi-point constraints (spider joints) using kinematic coupling (or rigid coupling, an RBE2 constraint in Nastran®), were placed at each of the three interfaces between the spring steel insert and the beams. Hurty/Craig-Bampton (HCB) reduction [13, 14] was applied to reduce the joints to pairs of interface nodes. Equation (2) shows the basic equation of motion for a model where the nonlinear joint forces $\mathbf{F}_J(\mathbf{x}, \boldsymbol{\theta})$ are the only source of damping. The external forcing for the system is represented by $\mathbf{F}_p$.

$$\mathbf{M}\,\ddot{\mathbf{x}} + \mathbf{K}\,\mathbf{x} + \mathbf{F}_J(\mathbf{x}, \boldsymbol{\theta}) = \mathbf{F}_p. \tag{2}$$

From Eq. (2), the HCB method then partitions all of the matrices according to internal and boundary nodes as shown below.

$$\begin{bmatrix} \mathbf{M}_{BB} & \mathbf{M}_{BI} \\ \mathbf{M}_{BI} & \mathbf{M}_{II} \end{bmatrix} \begin{Bmatrix} \ddot{\mathbf{x}}_B \\ \ddot{\mathbf{x}}_I \end{Bmatrix} + \begin{bmatrix} \mathbf{K}_{BB} & \mathbf{K}_{BI} \\ \mathbf{K}_{BI} & \mathbf{K}_{II} \end{bmatrix} \begin{Bmatrix} \mathbf{x}_B \\ \mathbf{x}_I \end{Bmatrix} + \begin{Bmatrix} \mathbf{F}_J(\mathbf{x}, \theta) \\ 0 \end{Bmatrix} = \begin{Bmatrix} \mathbf{F}_B \\ \mathbf{F}_I \end{Bmatrix} \tag{3}$$

Equation (3) has boundary degrees of freedom represented by *B* and internal degrees of freedom (DOF) represented by *I*. This then allows for the conversion of internal nodes to fixed-interface modal coordinates and then high frequency modes can be truncated to reduce the size of the system.

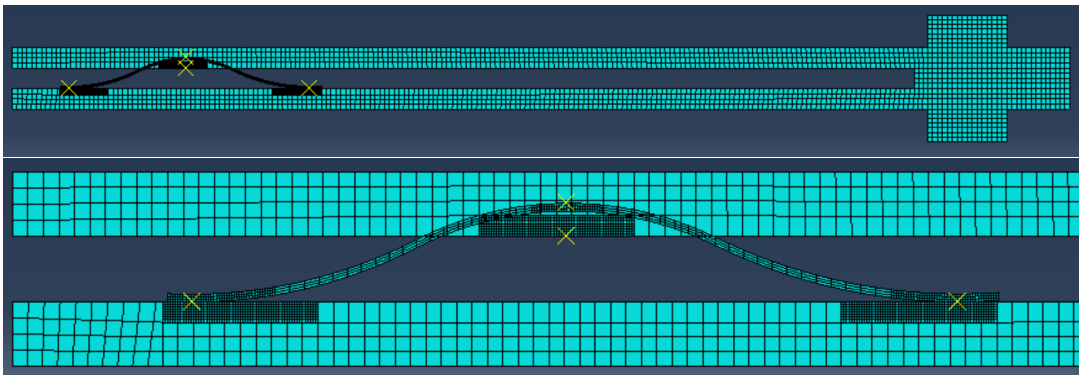

Figure 5: The mesh of the 2D FEM of the finger-seal test stand that was created in Abaqus. The yellow X's are the interface nodes that were retained in the ROM.

The linear model seeks to capture the linear stiffness behavior of the system by inserting linear springs in the x-translation, y-translation, and z-rotation directions. The same three spring stiffness values are used at all three joints. The mass and stiffness matrices were imported into MATLAB to create the linear model. A two-step optimization process was used, as detailed in Table 1, employing the MATLAB *fminsearch* function. Only the first three modes were used in this process, because Modes 4 and 5 are torsional modes that cannot be captured by a 2D model.

Table 1: Values assigned to spring constants in each step of the optimization process. Values denoted "optimize" are solved for in that step.

Step	**X**	**Y**	$\mathbf{R}_Z$
1 (slipping)	0	optimize	optimize
2 (stuck)	optimize	step 1 value	step 1 value

Table 1 shows the DOF values and experimental data used in each step of the optimization process. The first step finds the spring constants K_Y and K_{Rz} that best reproduce the modes of the system when the joint slips, hence the natural frequencies used in that step are those when the finger seal is slipping completely, which are extracted from Figs. 8, 9, and 10 as described subsequently. In the second step the optimization uses the linearized low-amplitude frequencies or stuck frequencies, which were either those from the low-amplitude data in Figs. 8, 9, and 10, or the linear test described in Section 2.1, to find the axial stiffness K_X. The average of the data in high-amplitude and in the low-amplitude regions, respectively, was used to define the stuck and slipping natural frequencies.

A 4-parameter Iwan element was then inserted between the interface nodes in the slip direction (x-direction) to capture the nonlinear behavior due to friction. Then the quasi-static modal analysis method [7] was used to capture the amplitude dependent frequency and damping of the modes of interest. In each case the linear springs are used between the Y and R_Z DOF, with the

stiffness values identified in Step 1. The four Iwan parameters were varied manually to find the optimal values to match the amplitude dependent frequency and damping of each mode to the nonlinear experimental data.

3 Results

Experimental results were obtained for several modes and are presented for the first 5 modes of the system; this includes two torsion modes, Modes 4 and 5, which were not present in the 2D FEM, and yet their results are interesting and are presented to explain the dynamics of the system and to enable future modeling.

3.1 Linear Experimental Results

The natural frequencies and damping ratios found from linear testing are shown in Table 2. The data with the seal was presumed to be capturing the low-amplitude micro-slip state of the test structure with the seal inserted. This is because the small hammer was unlikely to excite the system to a high enough amplitude to enter macro-slip. In addition, the data appeared to be linear with frequency shifts of only a few Hertz between hammer hits.

Table 2: Natural frequencies and damping ratios with and without the seal inserted from the linear testing

Mode	**Shape Descrip.**	**Natural Frequency (Hz)**		**Damping Ratio**	
		No Seal	**With Seal**	**No Seal**	**With Seal**
1	BS1	118	650	0.0006	0.0043
2	BA1	524	744	0.0016	0.0080
3	BS2	740	817	0.0012	0.0045
4	T1	907	984	0.0005	0.0045
5	T2	1091	1375	0.0010	0.0022

Adding the seal to the test structure added damping, as is shown Table 2 comparing the no seal and with seal damping ratios. The seal caused the low-level damping to increase by a factor ranging from 2-7. Additionally, note how the seal caused an increase in the system's linear natural frequencies. The seal causes the first mode to increase by almost six times, and it also causes significant stiffening in the other modes.

Table 3: Results from tests with various seal directions and orientations. Values given are the modal natural frequencies in Hz for Test 1 and the change in the frequency in Hz for Tests 2-7. Tests 3 and 4 are repeats of Tests 1 and 2 to evaluate repeatability.

Test	**Mode 1**	**Mode 2**	**Mode 3**	**Mode 4**	**Mode 5**	**Seal Direction**	**Orientation**
1	650	744	817	984	1375	Down	-
2	0.62	-6.18	10.77	-2.54	0.65	Up	-
3	0.00	0.54	0.12	-0.61	0.15	Down	-
4	0.92	-5.51	12.12	-1.93	0.65	Up	-
5	0.92	-5.65	13.10	-1.12	0.65	Up	Shift Left
6	-5.38	0.40	4.41	-2.54	0.15	Down	Shift Down
7	-2.15	-8.20	-0.49	-2.95	0.36	Down	Shift Up

The linear testing was repeated after repositioning the seal in various ways to evaluate the repeatability of the system. Table 3 shows the results of these tests. Notice that in Table 3, changing the direction of the seal in Tests 1-4 caused obvious and repeatable shifts in the natural frequencies. This demonstrates the significant influence that the direction of the seal has on the dynamics of the system. Table 3 also shows that shifting the seal to the left caused shifts of less than 1 Hz in the frequencies of Modes 3 and 4 and even smaller shifts in Modes 1, 2 and 5. This reveals that the system is not very sensitive to the lateral positioning of the seal. In contrast, shifting the seal down decreased the frequencies of Modes 1 and 4 by 5.38 Hz and 2.54 Hz, respectively, while increasing the frequency of Mode 3 by 4.41 Hz, with small changes to Modes 2 and 5. Shifting the seal up caused an even larger effect with slightly different patterns in the modes that were affected.

In Fig. 6, the hit point locations are shown that correspond to the X's in Fig. 3. Points 31-34 are the locations of the accelerometers and were not included in the mode shapes because there were no hammer hits at those locations.

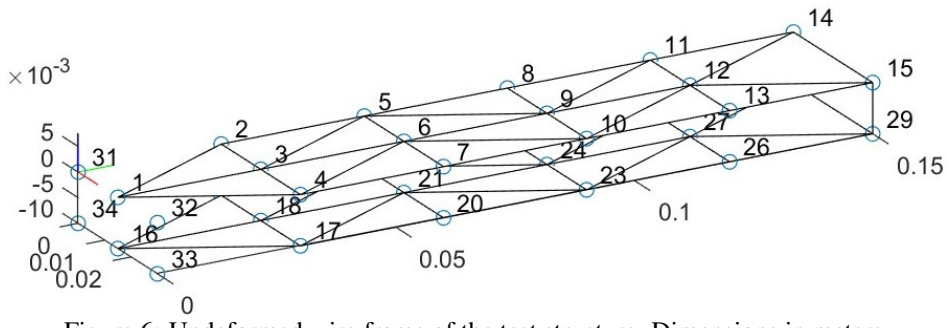

Figure 6: Undeformed wire frame of the test structure. Dimensions in meters.

The FRFs were fit using the AMI algorithm, and the mode shapes obtained at each hammer point, for the case where the seal was removed, are shown in Fig. 7. The mode shapes obtained for Modes 1-3 for the test data with the seal inserted were noisy, so they were not displayed here. This was investigated, and it was found that the natural frequency of these modes shifted slightly from one hammer hit to the next, so that when the set of FRFs was fit all at once, the shape would become highly distorted. Modes 4 and 5 with the seal inserted resembled those shown in Fig. 7. In contrast, if the FRFs from one hit and all four accelerometers were processed, the shape would come out clean and agree with the results above, at least at the four accelerometer locations. This justified the use of Equations (1a)-(1d) to accentuate the modes when processing the nonlinear measurements.

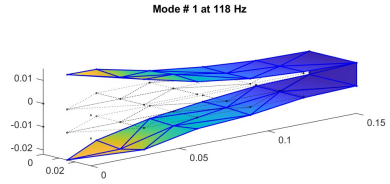

(a) Mode 1 - symmetric clapping mode

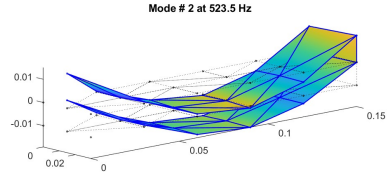

(b) Mode 2 - asymmetric bending mode

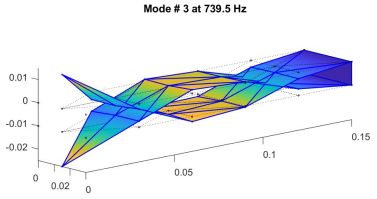

(c) Mode 3 - second symmetric bending mode

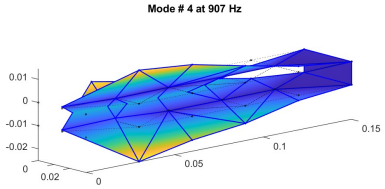

(d) Mode 4 - first torsional mode

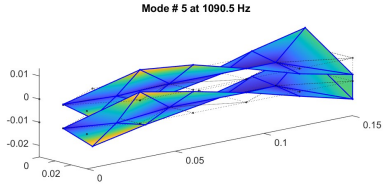

(e) Mode 5 - second torsional mode

Figure 7: Mode shapes 1–5 of the test structure without the seal.

One can use shapes to infer that hammer hits along points 2-4 and 17-19 line up with the node line for bending Mode 2 in Fig. 7b, and hence would cause minimal excitation of Mode 2. Indeed, when excited at these points, we obtained measurements that were clear outliers for Mode 2. In addition, hammer hits along the center line of the test article did not excite the torsional modes (Figs. 7d and 7e) effectively, so only hammer hits along the edges were used to obtain data for those modes.

3.2 Nonlinear Experimental Results

The nonlinear frequency and damping for Modes 1-5 were extracted from several hammer impacts for each mode, and are shown in Figs. 8 to 11. The linear natural frequencies from Table 2 were used as guides for setting the bounds for the band pass filter in finding the non-linear natural frequencies. It was assumed that the linear testing with the seal inserted would be comparable to the structure in micro-slip because small enough impacts were used to likely not cause the structure to enter macro-slip. The frequencies measured without the seal were expected to be comparable to those measured when the seal was

in macro-slip. One can compare these results with the frequencies in Tables 2 and 3 to verify this.

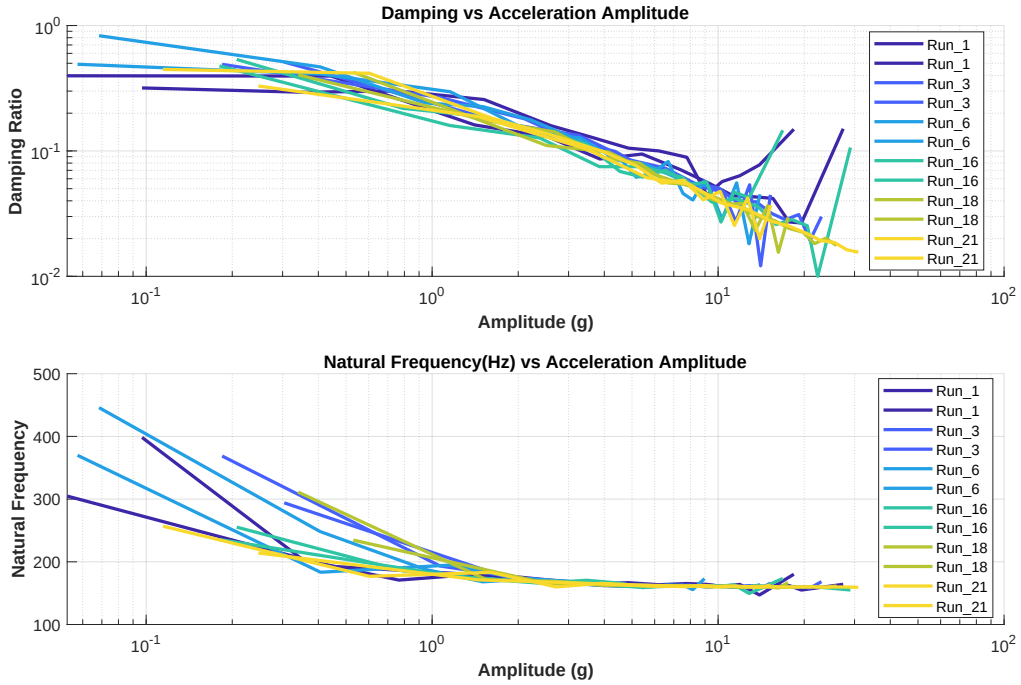

Figure 8: Effective natural frequency and damping ratio for Mode 1 in Fig. 7a obtained from hammer impacts with the medium hammer at various locations. The numbers on the legend refer to the hit point used to excite the test structure.

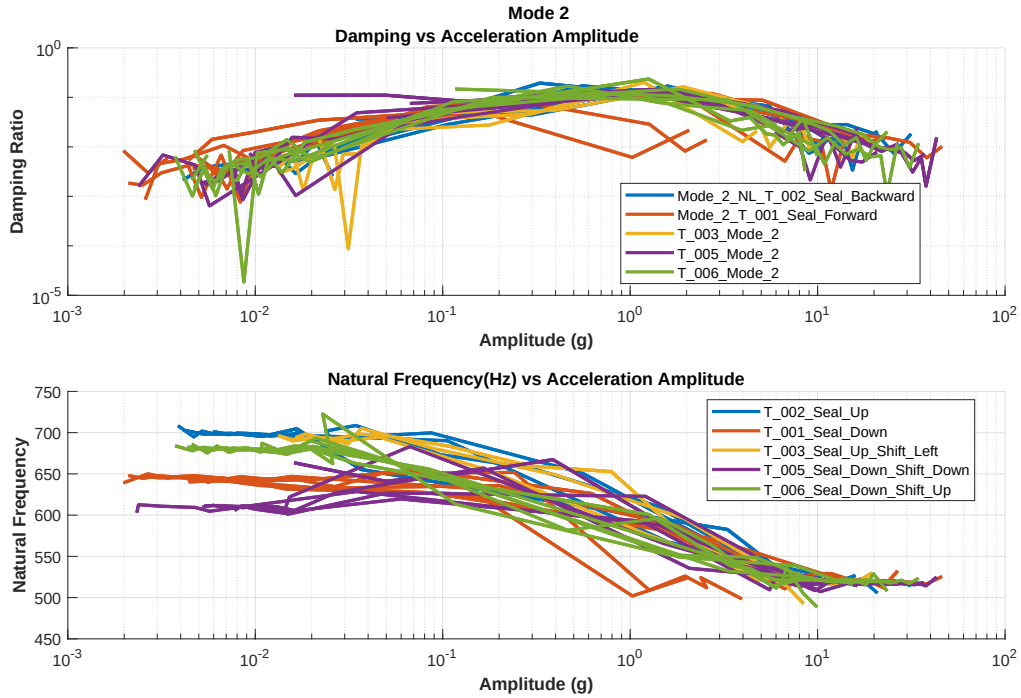

Figure 9: Effective natural frequency and damping ratio for Mode 2 in Fig. 7b obtained from impacts with the medium hammer at various locations. Results are shown for the five seal positions listed in Table 3.

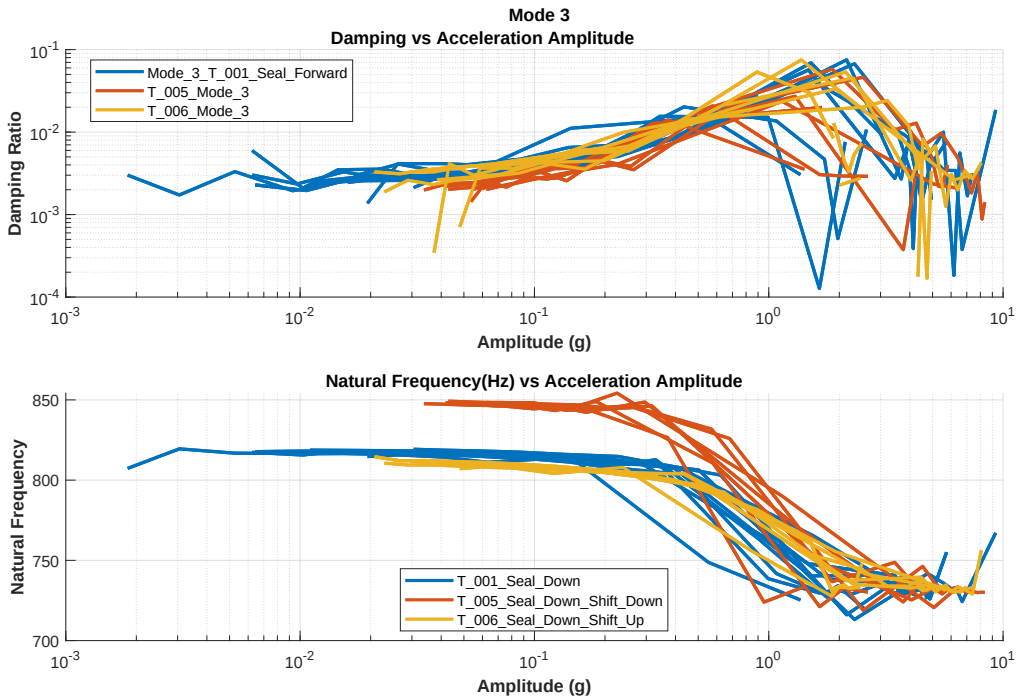

Figure 10: Effective natural frequency and damping ratio for Mode 3 in Fig. 7c obtained from hammer impacts with the medium hammer at various locations. Results are shown for three of the seal positions listed in Table 3.

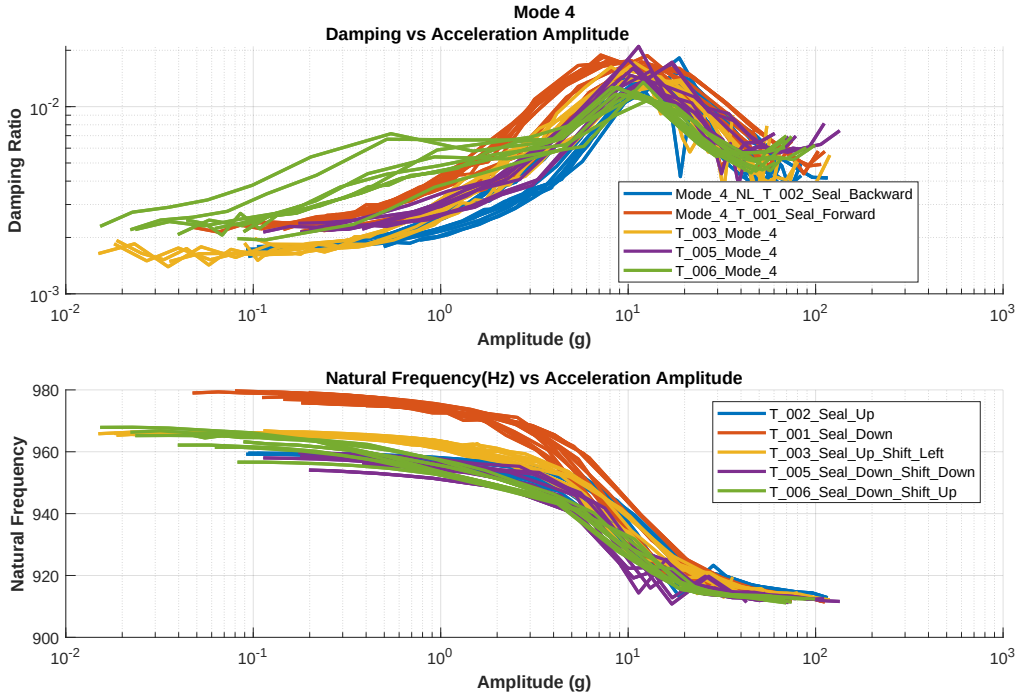

Figure 11: Effective natural frequency and damping ratio for Mode 4 in Fig. 7d obtained from hammer impacts with the medium hammer at various locations. Results are shown for five of the seal positions listed in Table 3.

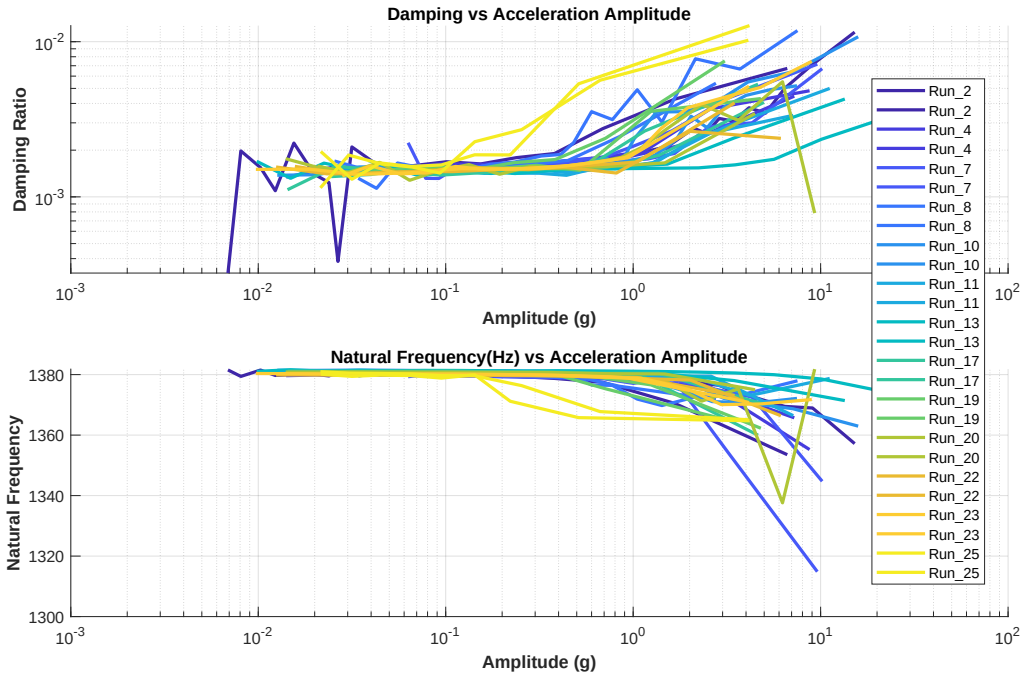

Figure 12: Effective natural frequency and damping ratio for Mode 5 in Fig. 7e obtained from hammer impacts with the medium hammer at various locations. The numbers in the legend refer to the hit point used to excite the test structure.

The effect of shifting the seal on the nonlinear modal behavior is also shown for Modes 2-4 in Fig. 9-11. Varying the seal location did not cause large changes in the macro-slip frequencies, but it did cause noticeable changes in the micro-slip frequencies. Focusing on Fig. 9, note how changing the seal direction from down to up caused an increase in micro-slip frequency of about 50 Hz and shifting the seal left had minimal impact on the micro-slip frequency of the system. Figure 10 does not include the data from the tests with the seal facing up because Mode 3 could not be captured in the micro-slip regime from those tests.

3.3 Discussion on Experimental Results

These studies show how much one can expect the dynamics of this test stand to change due to variations in the manufacturing and orientation of the finger seal. The damping ratio changed minimally with seal orientations across the modes. The low-amplitude natural frequency changed with the seal orientation, by as much as 15%. The tests are quite repeatable across different nominally identical tests, and even the worst case changes are relatively small relative to the overall nonlinearity in each mode. Hence, with moderate care in controlling the position and orientation of the seal, one should be able to obtain repeatable results. Note that the results for Modes 1 and 5 in Figs. 8 and 12 do not include data where the seal position varied. That data did not show a clear effect on the nonlinear results, and so it was omitted.

The full transition between micro-slip and macro-slip was captured for Modes 2-4. For these modes the frequency and damping started with a near zero slope, suggesting a low-amplitude asymptote. In contrast, only the higher amplitude slipped state is captured for Mode 1, as shown in Fig. 8. It appears that the clapping motion of Mode 1 is rapidly damped as the amplitude of this mode decreases, so that too few cycles are obtained in the stuck configuration for the Hilbert transform to extract that state from the measurements. It is also possible that the response of Mode 1 tends towards more than one asymptote, depending on where the system sticks. The macro-slip state for Mode 5 does not appear to have been captured, presumably because the forces used were not sufficient to excite high enough amplitudes to cause the joint to fully slip for that mode.

3.4 Reduced Order Model

Spiders were placed at the three contact points between the seal and the beams. Linear springs were inserted at each of the spiders and optimized to align the micro-slip and macro-slip frequencies for the linear model with the experimental results, as outlined in Table 1. The slipping frequency for Mode 1 was taken from Fig. 8 at high amplitude; Mode 1's stuck frequency was treated as unknown because that frequency could not be deduced from the nonlinear data in Fig. 8. The micro-slip and macro-slip frequencies used for Modes 2 and 3 were taken from test T_001_Seal_Down (see Figs. 9 and 10). We found that

considering both stuck and slipping states in the optimization improved the correlation between the model and the linear and nonlinear measurements. The stiffness parameters obtained by the optimization procedure are shown in Table 4, and the resulting stuck and slipping natural frequencies are shown in Table 5.

Table 4: Stiffness Parameters Obtained from Optimization

DOF	**Stiffness Parameter (lbf/in)**
X	2,000,000
Y	1,200
RZ	2

Table 5: Comparison of the ROM natural frequencies with those from the experiments in both macro-slip and micro-slip.

	Macro-Slip Frequencies (Hz)			**Micro-Slip Frequencies (Hz)**		
Mode	**Experimental**	**Model**	**Percent Error**	**Experimental**	**Model**	**Percent Error**
1	160	188	17.3	-	390	-
2	520	507	-2.5	650	643	-1.1
3	730	735	0.7	820	796	-3.0

Table 6: Iwan Parameters

FS	**Kt**	**Chi**	**Beta**
0.010 lbf	2.0×10^{6} lbf/in	-0.80	2.0

The Iwan parameters of the joints were then manually adjusted until the ROM reproduced the nonlinear behavior of Modes 1-3 as accurately as possible. The resulting Iwan parameters are given in Table 6, and those were then used in the ROM to find the frequency and damping of each mode as a function of vibration amplitude. The results for Modes 1-3 are shown in Figs. 13-15.

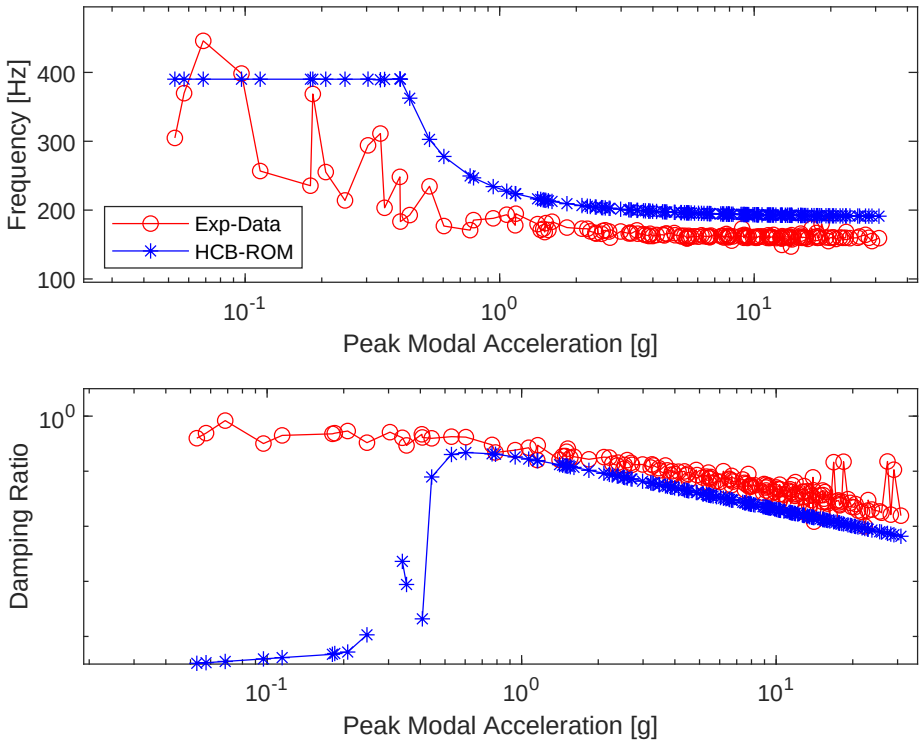

Figure 13: Natural frequency and damping of Mode 1 of the ROM compared to the experimental measurements.

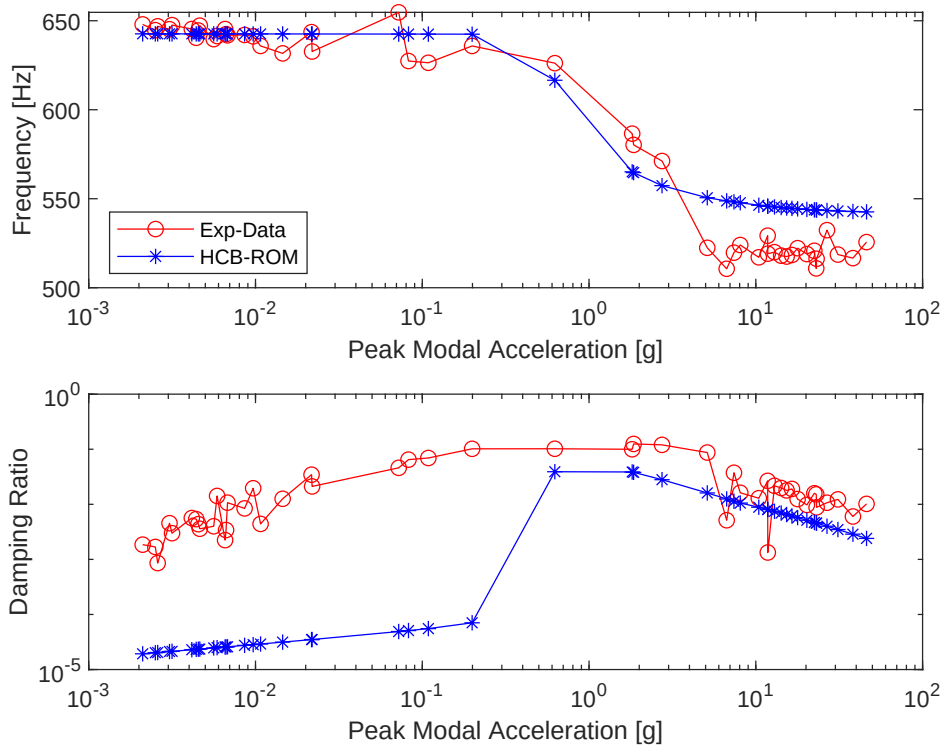

Figure 14: Natural frequency and damping of Mode 2 of the ROM compared to the experimental measurements.

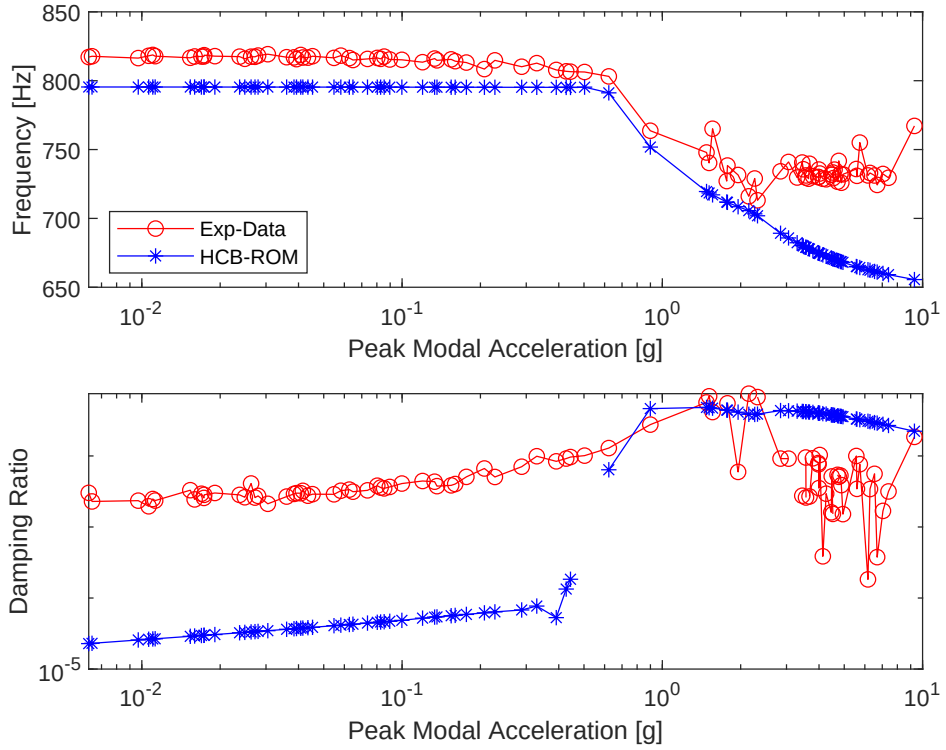

Figure 15: Natural frequency and damping of Mode 3 of the ROM compared to the experimental measurements.

3.5 ROM Discussion

The results for each mode show that the ROM predicts a very low damping ratio at low-amplitudes, which then transitions suddenly to the macro-slip damping. The experimental data does not show this behavior, but exhibits frequencies that decrease smoothly and damping that also evolves smoothly. This is especially evident in Mode 1, which transitions suddenly from macro-slip to micro-slip at an acceleration of 0.5 g. This was investigated and did not seem to be an issue with convergence of the simulations, but to be an actual change in the behavior of the ROM as the first finger seal interface slips. The experimental results for Mode 1 showed a large amount of variation at low amplitudes, so it is unclear how much the model should be expected to follow that data. It is also important to note that Modes 1 and 3 are symmetric modes, and so they might exhibit bilinear behavior. Quasi-static modal analysis is not necessarily expected to work well for a bilinear system, because Masing's rules don't apply there and often the bilinearity produces a very small change in the mode frequency with vibration amplitude, while producing large asymmetry in the time response [15, 16, 17]. Hence, it is encouraging that the the damping was captured reasonably well for all three modes.

Mode 2 is a symmetric bending mode, and so its nonlinearity is dominated by axial slip at the interfaces between the finger seal and beams. This is the type of nonlinearity exhibited in our prior works [7, 18], and so we would expect this modeling strategy to work well for this mode. The frequency of this mode is predicted well, but the damping once again is greatly under-predicted in micro-slip. It should also be noted that the QSMA prediction does not converge to 507 Hz at high amplitude, which is the theoretical macro-slip frequency in Table 5. This was investigated and seems to be an inaccuracy in QSMA, which comes about because the mode shapes of this system change quite substantially as the system transitions into macroslip. The error at high amplitudes could be addressed by using the Rayleigh Quotient (RQMA) approach, which is akin to QSMA but allows the mode shapes to change [19]. Mode 3 also seems to exhibit this inaccuracy. In contrast, the linear frequencies for Mode 1 in Table 5 match the frequencies exhibited by the ROM in Fig. 13 very closely.

4 Conclusion

In this study, a simple test article was created that mimics the dynamics that a finger seal might exhibit in a turbine engine. Impact testing was used to capture the linear and nonlinear responses of the first five modes of the structure. The Hilbert transform, along with a modal filter, allowed for the capture of natural frequency and damping of each mode of the system across a range of amplitudes. The test article was found to exhibit a range of behaviors from micro-slip through macro-slip even when subjected to a relatively small range of forces. Hence, this system may be of interest for general studies of the nonlinear dynamics of systems with friction. The low- and high-amplitude behaviors of the structure seemed to exhibit the characteristics expected for micro-slip and macro-slip, respectively, for 3 of the 5 modes investigated. It was shown that the micro-slip frequencies were sensitive to changes in the seal's location and orientation, while the macro-slip frequencies were not.

Linear and Nonlinear reduced-order models were created and tuned to capture the dynamics of the finger seal structure. They were found to effectively capture the transition in the natural frequency from micro-slip to macro-slip and the high-amplitude damping of the system was predicted reasonably well. On the other hand, the ROM showed too abrupt of a transition from micro- to macro-slip, and the reason for this is not known. Further testing would be helpful, for example to very accurately measure the dimensions of the seal and hence to understand why its orientation changed the results so much. Efforts are also underway to refine the ROM, for example by using different Iwan elements at the various interfaces, which seems reasonable because the contact pressures are different at each.

Acknowledgments

The authors are grateful to Pratt and Whitney for helpful discussions and for providing the motivation to pursue this system.

References

[1] **Chuong, C.** and **BUDNICK, M.**, *United States Patent: Gas turbine seal assembly and seal support*, Jul. 2014.

[2] **BUDNICK, M.**, *United States Patent: Multi-ply finger seal*, Sep. 2014.

[3] **Chupp, R. E., Hendricks, R. C., Lattime, S. B.** and **Steinetz, B. M.**, *Sealing in Turbomachinery*, Journal of Propulsion and Power, Vol. 22, No. 2, pp. 313–349, Mar. 2006.

[4] **Brake, M., Allen, M., Quinn, D., Roettgen, D.** and **Nowell, D.**, *Testing and Modeling of Friction and Slip in Mechanical Interfaces: State of the Art and Perspectives for the Next Decade.*, Journal of Structural Dynamics, 2024, publisher: University of Liege.

[5] **Mathis, A. T., Balaji, N. N., Kuether, R. J., Brink, A. R., Brake, M. R. W.** and **Quinn, D. D.**, *A Review of Damping Models for Structures With Mechanical Joints1*, Applied Mechanics Reviews, Vol. 72, No. 040802, Jul. 2020.

[6] **Segalman, D. J., Gregory, D. L., Starr, M. J., Resor, B. R., Jew, M. D., Lauffer, J. P.** and **Ames, N. M.**, *Handbook on Dynamics of Jointed Structures*, Tech. Rep. SAND2009-4164, Sandia National Laboratories, Albuquerque, NM 87185, 2009.

[7] **Lacayo, R. M.** and **Allen, M. S.**, *Updating Structural Models Containing Nonlinear Iwan Joints Using Quasi-Static Modal Analysis*, Mechanical Systems and Signal Processing, Vol. 118, No. 1 March 2019, pp. 133–157, 2019, number: 1 March 2019.

[8] **Singh, A., Wall, Mitchell, Allen, Matthew S.** and **Kuether, Robert J.**, *Spider Configurations for Models with Discrete Iwan Elements*, *Nonlinear Structures and Systems*, Vol. 1, pp. 25–38, Springer, Orlando, Florida, Jan. 2019.

[9] **EL-Aini, Y. M., Benedict, B. K.** and **Wu, W.-T.**, *Friction Damping of Hollow Airfoils: Part II—Experimental Verification*, Journal of Engineering for Gas Turbines and Power, Vol. 120, No. 1, pp. 126–130, Jan. 1998.

[10] **Magoffin, Sean, Smith, Eli** and **Allen, Matthew S.**, *Design and Quasi-Static Modal Analysis to Predict Nonlinear Behavior of a Finger Seal*, *The 44th International Modal Analysis Conference (IMAC-XLIV)*, Palm Springs, CA, USA, Jan. 2026.

[11] **Gilbert, Suzanna, Allen, Matthew S.** and **Rapp, Brandon**, *Nonlinear System Identification of a Riveted Beam using a Hilbert Transform Based Approach*, *43rd International Modal Analysis Conference (IMAC XLIII)*, Orlando, FL, Feb. 2025.

[12] **Feldman, M.**, *Non-linear system vibration analysis using Hilbert transform–I. Free vibration analysis method 'Freevib'*, Mechanical Systems and Signal Processing, Vol. 8, No. 2, pp. 119–127, 1994.

[13] **Hurty, W. C.**, *Dynamic analysis of structural systems using component modes*, AIAA Journal, Vol. 3, No. 4, pp. 678–685, Apr. 1965, number: 4.

[14] **Craig, R. J.** and **Bampton, M.**, *Coupling of Substructures for Dynamic Analysis*, AIAA Journal, Vol. 6, No. 7, pp. 1313–1319, 1968, number: 7.

[15] **Caughey, T. K.**, *Random excitation of a system with bilinear hysteresis*, J. Appl. Mech., Vol. 27, No. 4, pp. 649–652, 1960.

[16] **Pacini, B. R., Holzmann, W. A.** and **Mayes, R. L.**, *Performance of Nonlinear Modal Model in Predicting Complex Bilinear Stiffness*, *Nonlinear Dynamics, Volume 1*, edited by Kerschen, G., Conference Proceedings of the Society for Experimental Mechanics Series, pp. 101–112, Springer International Publishing, Cham, 2019.

[17] **Ondra, V., Sever, I.** and **Schwingshackl, C.**, *A method for non-parametric identification of non-linear vibration systems with asymmetric restoring forces from a resonant decay response*, Mechanical Systems and Signal Processing, Vol. 114, pp. 239–258, 2019, publisher: Elsevier, Bilinear.

[18] **Zare Estakhraji, S. I., Wall, M., Capito, J.** and **Allen, M. S.**, *A thorough comparison between measurements and predictions of the amplitude dependent natural frequencies and damping of a bolted structure*, Journal of Sound and Vibration, Vol. 544, pp. 117397, Feb. 2023.

[19] **Balaji, N. N.** and **Brake, M. R.**, *A quasi-static non-linear modal analysis procedure extending Rayleigh quotient stationarity for non-conservative dynamical systems*, Computers & Structures, Vol. 230, pp. 106184, Apr. 2020.